Emergence of dynamic phases in the presence of different kinds of open boundaries in stochastic transport with short-range interactions

Hannes Nagel and Wolfhard Janke

Institut für Theoretische Physik, Universität Leipzig, Postfach 100 920, 04009 Leipzig, Germany

E-mail: Hannes.Nagel@itp.uni-leipzig.de and Wolfhard.Janke@itp.uni-leipzig.de

Abstract. We discuss the effects of open boundary conditions and boundary induced drift on condensation phenomena in the pair-factorized steady states transport process, a versatile model for stochastic transport with tunable nearest–neighbour interactions. Varying the specific type of the boundary implementation as well as the presence of a particle drift, we observe phase diagrams that are similar but richer compared to those of the simpler zero-range process with open boundary conditions. Tuning our model towards zero-range-process-like properties we are able to study boundary induced effects in the transition regime from zero-range interactions to short-range interactions. We discuss the emerging phase structure where spatially extended condensates can be observed at the boundaries as well as in the bulk system and compare it to the situation with periodic boundaries, where the dynamics leads to the formation of a single condensate in the bulk.

Keywords: driven diffusive systems (theory), free boundary problems (theory), stochastic particle dynamics (theory)

Contents

1. Introduction

Stochastic mass transport processes such as the asymmetric simple exclusion process (ASEP) or the zero-range process (ZRP) proposed by Spitzer [1] are simple transport models for particle hopping aiming to improve the understanding of basic phenomena in the dynamics of particles in driven diffusive systems. Generally, these particles are abstract and may represent objects from the microscopic to the macroscopic scale when combined with appropriate dynamics. It is this relation of abstract particles and a multitude of different kinds of dynamics that generates manifold mappings to physical processes and phenomena. One such phenomenon that is of particular interest to us, is the formation of particle condensates. In fact, dynamics leading to steady states in closed, periodic systems where particles form condensates have been studied already for the ZRP [1–9] as well as for processes with short-range interactions [10–12]. On inhomogeneous structures such as a star graph or scale-free networks even the most simple dynamics of uniform hopping can lead to condensation at the inhomogeneities [13–15]. On a homogeneous structure, condensates can emerge anywhere in the system as long as the interaction potential falls off sufficiently fast [10]. For a general overview of stochastic transport processes and condensation phenomena we refer the reader to the reviews by Schütz [16] and Evans and Wacław [20, 21] or the book by Schadschneider et al [17].

While the ZRP as well as the extended models can be considered to be driven far from equilibrium, their steady state that leads to the condensation remains the same as in equilibrium. In fact, in the case of systems with periodic boundaries with particle conservation, they are constructed to have this property. This is, however, not a general property of transport processes, as can be seen in the exclusion model of Katz, Lebowitz and Spohn [18, 19] where the stationary distribution may or may not depend on the external field depending on the interaction parameters of the model. It is, however, also of interest to understand the changes to the condensation process when this steady state is broken by replacing the periodic with open boundaries through which particles can enter or leave the system, thereby creating a current. In general, this external drive and current can lead to phase separation [22]. In fact, for the ZRP, a specific study has been performed by Levine *et al* [23], were among other results phase separation due to the introduced boundary drive has been observed. In this paper we seek to extend this approach to a stochastic transport process with short-range interactions that feature spatially extended condensates in its steady state. This is of interest to us because, in contrast to the ZRP, such an extended process is able to interact with the boundary due to its non-zero interaction range. As a consequence we are forced to discuss different types of open boundaries to grasp their effects on possible condensate formation and dynamic phases. Also, instead of using a simpler transport process with short-range interactions such as proposed by Evans *et al* [10], we decided to employ a tunable model [11, 12] that can be parameterized to resemble the condensation properties of the ZRP as well as extended condensates such as those considered in [10]. This allows us to compare properties of this model to those of the ZRP discussed in [23] before going into detail with different types of boundaries. Because the short-range interactions in that class of transport processes are strongly related to the fact that the steady state of a closed system factorizes over pairs of adjacent sites, we will sometimes use the term *pair-factorized steady states (PFSS) model*, although with open boundaries a steady state does not necessarily exist. In a previous short note [24], we have already briefly discussed emerging phases and effects caused by the driven open boundaries. We did, however, consider only one specific type of open boundary and were severely limited by the employed numerical method. In a recent short communication [25], we sketched an improved simulation setup and discussed for this special case the phase diagram and transition dynamics between the phases in more detail. In particular, we pointed out that not only the details but, in fact, the very existence of phases depends on the choice of interaction with the boundary. We would, therefore, like to complete the picture with that versatile numerical approach and an emphasis on the point that the specific interaction details at the boundaries have significant impact on the system's phase diagram.

The remainder of this paper is organized as follows. In the next section we will briefly introduce the zero-range process as well as the tunable short-range interaction stochastic transport model and define the considered types of open boundaries. In the third section we describe the used numerical methods and motivate our choice for a kinetic Monte Carlo algorithm. In the fourth section we will discuss our results, first making a comparison with the zero-range process and then discussing emerging phases and properties in detail with short-range interactions turned on. Finally, we summarize our findings in the fifth section.

3

2. Stochastic transport processes with open boundaries

The basic particle-hopping stochastic transport process consists of a one-dimensional lattice with L sites and a gas of M indistinguishable particles. Each site i of the lattice can be occupied by any number $m_i = 0, ..., M$ of particles, where $M = \sum_{i=1}^{L} m_i$ is the total number of particles. These particles can leave their sites i with a rate u_i and then jump to one of the adjacent sites. A target site is randomly selected among the neighbours with respect to the strength of asymmetric hopping given by the parameters p and q so that the actual rates of particles hopping to the sites right $(i + 1)$ and left $(i - 1)$ of the departure site become pu_i and qu_i, respectively, as indicated in figure 1. At the boundaries, particles enter or leave the system. We define exchange rate parameters p_{in}, q_{in} and p_{out}, q_{out} to control particle currents into and out of the system. The exact mechanisms of injection and removal of particles at the boundaries are discussed further below where we define the specific properties and implementations of the boundaries.

2.1. Zero-range process

The hopping rate function u_i determines the dynamics of the particles in the system. For zero-range processes it must depend only on the occupation number of the departure site which results in a local-only interaction term. An example for a specific ZRP, that is of particular interest in the context of this work, is the condensation model with hopping rates

$$u(m) = 1 + b/m, \tag{1}$$

where a single-site particle condensate spontaneously emerges for $b > 2$ in the steady state of the periodic system when the particle density exceeds the critical density $\rho_{\mathrm{crit,ZRP}} = 1/(b - 2)$ [26].

2.2. PFSS process

In this paper, we consider a more generic model where the hopping rate function depends also on the number of particles on the adjacent sites as proposed by Evans *et al* [10]. With an appropriate choice of the hopping rate function, spatially extended condensates emerge in the periodic system due to the nearest–neighbour interaction. One generic choice of the hopping rate function of this process reads

$$u_i = \prod_{\langle i,j \rangle} u(m_i, m_j) = \prod_{\langle i,j \rangle} \frac{g(m_i - 1, m_j)}{g(m_i, m_j)}, \tag{2}$$

making the interaction potentials between adjacent sites $\langle i, j \rangle$ sites isotropic for symmetric weight functions $g(m, n) = g(n, m)$. By construction this results in a pair-factorized steady state probability distribution of the form

$$P_{M,L}(\{m\}) = Z_{M,L}^{-1} \prod_{\langle i,j \rangle} g(m_i, m_j) \delta_{\sum_{i=1}^{L} m_i, M}, \tag{3}$$
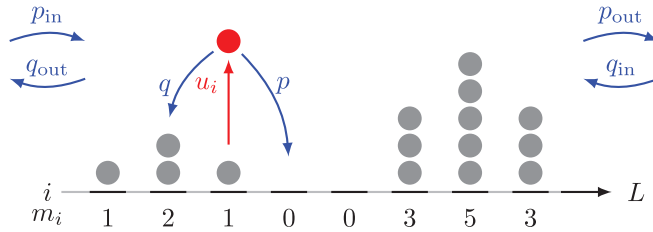
Figure 1. Schematic representation of the dynamics of a particle hopping process on a one-dimensional lattice with L sites, hopping rate u_i and drift parameters p, q. At the boundary sites, the drift parameters towards the boundary are replaced with the removal parameters p_{out} and q_{out} as indicated. Likewise, the rate of particle injection at the boundaries is given by the parameters p_{in} and q_{in}, respectively.

as long as the number of particles is conserved. Here $\{m\}$ gives a complete state, $Z_{M,L}$ normalizes the steady state similar to the partition function in an equilibrium system and the Kronecker symbol fixes the particle number.

To be able to compare to the work on ZRP with open boundaries [23] as well as to consider a process with effective long-range interactions, we use the hopping rate function generated by the tunable interaction terms

$$g(m, n) = \exp\left[-|m - n|^{\beta} - \frac{1}{2}(m^{\gamma} + n^{\gamma})\right] \tag{4}$$

proposed by Wacław *et al* [11, 12]. The weights $g(m, n)$ consist of a zero-range interaction term tuned by the parameter γ and a nearest–neighbour interaction term tuned by the parameter β. The steady state of this process features the formation of particle condensates of various properties depending on the values of these parameters. A critical density and thus condensation phenomena exists for $0 \leqslant \gamma \leqslant 1$. The condensate then assumes one out of three qualitatively distinct forms that strongly influences the model's dynamics: a single-site peak for $\beta < \gamma$, an extended rectangular shape for $\gamma < \beta < 1$ or a smooth parabolic shape for $\beta > 1$ [11, 12, 27]. Most important to our purpose is the ability to reproduce single-site condensates similar to those observed for the ZRP with hopping rates (1) for $\beta < \gamma$ and $\gamma \leqslant 1$, as well as spatially extended smooth condensates for $\beta > 1$ and $\gamma \leqslant 1$ similar to those observed in [10].

2.3. Open boundaries: mechanisms of particle exchange and external drive

For the zero-range process the implementation of open boundaries is straightforward because there is no interaction other than particle exchange. For the considered model (2)–(4), on the other hand, the type of interaction at the boundary sites $i = 1$ and $i = L$ has to be chosen explicitly due to its non-zero interaction range. We will consider and discuss two main types of implementations.

Our first approach is to interpret the system as isolated and discard the interaction terms of the bonds that cross the boundary as follows from the factorization of weights for arbitrary graphs in equation (2). In the following, we will refer to this type as *loose* boundaries. As a second approach we consider the system to be embedded in a larger system with a separation that hinders particle movement like a membrane. Here, we do not discard the interaction term for the bond that crosses the boundary as it reflects

the interaction with some mean-field occupation outside of the considered system by setting the external particle occupation to a constant value m_∞. In contrast to the first approach, we refer to this type with the term *fixed* boundaries. This results in the hopping rates

$$u_1, u_L = \begin{cases} u(m_1, m_2), & u(m_L, m_{L-1}) & \text{for } \textit{loose} \text{ boundaries,} \\ u(m_1, m_2)u(m_1, m_\infty), & u(m_L, m_{L-1})u(m_L, m_\infty) & \text{for } \textit{fixed} \text{ boundaries.} \end{cases} \quad (5)$$

Additionally we consider two types of particle removal at the boundary sites that differ in the way the hopping rate determines the rate of particles leaving through the boundary. Intuitively, the rates of removal are $u_1 q_{\text{out}}$ at the first and $u_L p_{\text{out}}$ at the last site. This mechanism is used for the ZRP in [23] as well as in our own prior study [24]. Because normal hopping is involved for particles leaving the system, we use the term *hopping* removal to refer to this. Here, we also consider a second removal mechanism for particles that is symmetric to the mechanism of particles entering the system that occurs at a constant rate. For the latter mechanism we use the term *constant* removal. Because at the boundary sites the rate of particles leaving the system is decoupled from the hopping rate u_1 and u_L, we replace them with u_1^* and u_L^* and define

$$u_1^*, u_L^* = \begin{cases} u_1, u_L & \text{for } \textit{hopping} \text{ removal,} \\ 1, 1 & \text{for } \textit{constant} \text{ removal,} \end{cases} \quad (6)$$

so that the removal rates become $u_1^* q_{\text{out}}$ for the first and $u_L^* p_{\text{out}}$ for the last site. Rates of particles moving towards the bulk system remain unchanged ($u_1 p$ and $u_L q$, respectively).

In the following, we will consider only exchange rates that in general reflect the external drive of the system. That is, for symmetric dynamics ($p = q = 1/2$) the exchange parameters are identical at both boundaries ($p_{\text{in}} = q_{\text{in}}, p_{\text{out}} = q_{\text{out}}$), while for totally asymmetric hopping ($p = 1, q = 0$) the exchange is restricted to that spatial direction as well ($q_{\text{in}} = q_{\text{out}} = 0$).

3. Numerical simulation methods

The usual approach to simulating the dynamics of a stochastic transport process as a Markov chain is as follows: first propose a random departure site i, second compute the acceptance probability for the hop from the hopping rate u_i and third decide whether a particle hops to a randomly choosen neighbour. To compute an acceptance probability it is required, however, that the hopping rate function can be normalized for any permissible local combination of occupation numbers. This normalization basically results in a change of the simulation time scale by the normalization factor.

While this is possible both for hopping rate functions with an upper bound, such as equation (1) and those proposed by Evans *et al* [10], or when a maximum rate is known due to conservation of the total number of particles $M(t) = \text{const}$, it becomes inefficient

for increasingly separated intrinsic time scales of slow and fast events and thus results in a large ratio of rejected updates.

The hopping rates of the model considered here, however, do not have an upper bound in the regime $\beta > 1$. In fact, the required normalization constant would grow roughly as the square of the number of particles in the system, so that the approach to directly simulate the dynamics as sketched above cannot be used here. To work around this limitation as well as to improve efficiency in the presence of fast and slow events we employ a rejection-free kinetic Monte Carlo (KMC) algorithm introduced as the *direct method* by Gillespie [28, 29] for the simulation of coupled rate equations. While the method was designed for small chemical systems with few reactions, it can be made fit for efficient simulation of larger systems with some optimizations. The idea of the method is similar to those of other rejection-free KMC methods such as the n-fold way algorithm [30, 31] in that an update consists of selecting an event according to its specific rate Γ_k relative to the total rate $\Gamma = \sum_k \Gamma_k$ of all possible events, execute it and update the system time $t \to t + \Delta t$, where Δt is the waiting time to generate this event. Finally the list of possible events and their assigned rates Γ_k are updated to reflect the new state of the system. In the direct method, the event k is picked by the relation $\sum_{i=1}^{k-1} \Gamma_i \leqslant \Gamma x_1 < \sum_{i=1}^{k} \Gamma_i$ and the exponentially distributed time increment Δt is determined as $\Delta t = -(\ln x_2)/\Gamma$ using two uniformly distributed random numbers $x_1, x_2 \in [0, 1)$. For our model these events are all the particle transfers between adjacent sites $\langle i, j \rangle$ with their rates $u_i p, u_i q$ for $1 < i < L$, $u_1 p$, $u_L q$ and the removal and injection of particles at the boundaries with rates $u_1 q_{\mathrm{out}}, u_L p_{\mathrm{out}}$ and $p_{\mathrm{in}}, q_{\mathrm{in}}$, respectively.

The search for the appropriate event is easily improved by using a binary search tree [32] combined with multiple levels of search, where events that originate from the same site are grouped in the first search level, and then resolving to one specific event for that site. The step to update the rates of events is efficiently implemented by taking into account which events' rates actually need updating based on which neighbouring sites were involved in the last step of the Markov chain. This is basically an application of the proposed update principle of the next-reaction method [33] which involves building dependency graphs between events and rate recalculation to achieve this. As an additional advantage to simpler methods, the time scale of simulations becomes equivalent to the physical time scale, thus making it obsolete to define artificial time scales in terms of sweeps or local updates.

Because of the continuous time simulation method, we cannot compare CPU time per full update, but per unit physical time of the simulated system. For a lattice size of $L = 256$ sites, the simple simulation for the ZRP takes 31 μs, somewhat faster than the KMC method with 37 μs for one unit of model time. In a situation with slow and fast events, however, the simple method becomes slower proportional to the ratio of large to small rates, while the performance of the KMC method does not suffer from that. In our simulations the typical inprovement factor with only $M \approx 100$ would be around 50 but growing roughly with the square of the total particle number.

To compute the observables for the phase diagrams, we simulated at least 25 replicas for each point ($p_{\mathrm{in}}, p_{\mathrm{out}}$), and between 50 and 100 for points near the transition lines.

7

4. Results

4.1. Open boundary effects in the zero-range process like regime

We start the discussion of boundary drive induced dynamical phases with a look at the zero-range process with hopping rates (1). Most notably, for $b > 2$, it features spontaneous symmetry breaking and the formation of a single-site particle condensate in its steady state for periodic boundaries. That is, a single site contains a finite fraction $1 - \rho_{\mathrm{crit}}/\rho$ of all particles, where $\rho_{\mathrm{crit}} = 1/(b-2)$ is the critical density that is assumed on average in the rest of the system. Effects of open, driven boundaries on this model have been studied and discussed by Levine *et al* [23]. For the ZRP, we will use the parameter $b = 5$ that results in a critical density of $\rho_{\mathrm{crit}} = 1/3$. In the following we tune the coupling parameters β and γ of our model equation (4) to a regime where the condensation process with periodic boundary conditions has similar properties in the steady state as the ZRP and compare some of the properties to those found for the ZRP. With the choice of parameters $\beta = 0.4$ and $\gamma = 0.6$ in equation (4) a single-site condensate and critical density of $\rho_{\mathrm{crit}} = 0.302 \pm 0.006$ similar to that of the ZRP is expected for periodic boundary conditions [27]. We use *loose* boundaries with *hopping* removal, the latter of which is the same as that used for the ZRP in [23].

Two major phases are expected for the ZRP with open boundaries [23]. First, a steady state with a thin homogenous particle gas, and second, a phase with aggregate condensates formed at one or both boundaries that act as particle reservoirs and can influence the bulk system in between. To distinguish between these phases we measure time series of the total number of particles $M(t)$ and the bulk density ρ_{bulk}. It is useful to determine a scaling exponent α for $M(t)$ assuming it roughly follows a power-law $M(t) \sim t^{\alpha}$ to find the two phases. The bulk density is estimated as the average particle density in the bulk of the system

$$\rho_{\mathrm{bulk}} = \frac{1}{1 + i_{\mathrm{bl}} - i_{\mathrm{bf}}} \sum_{i=i_{\mathrm{bf}}}^{i_{\mathrm{bl}}} m_i, \text{where } m_i > 0 \ \forall \ i < i_{\mathrm{bf}} \text{ and } i > i_{\mathrm{bl}}, \quad (7)$$

that is, the region from the first (i_{bf}) to the last (i_{bl}) unoccupied site in the system.

From the plots of the scaling exponent α given in figure 2 as well as the bulk density ρ_{bulk} given in figure 3 we can clearly identify the same phases for this regime of our tunable model (4) as of the ZRP. In both models there is a particle gas phase (G) with a low stationary particle density $\rho \equiv \rho_{\mathrm{bulk}}$ that increases towards the transition line to the aggregate condensate phase (A). There, large numbers of particles aggregate at the first and/or last sites of the system. While the latter phase is homogeneous in systems with symmetric hopping ($p = q = 1/2$), sub-phases $\mathrm{A_{in}}$, $\mathrm{A_{out}}$ and A, where the aggregate condensate forms at the first site $i = 1$, the last site $i = L$, or both, can be identified for asymmetric hopping ($p \neq q$), see figures 2(b), (d) and 3(b), (d). The aggregate condensates at the boundary sites act as reservoirs for particles entering ($\mathrm{A_{in}}$) and leaving ($\mathrm{A_{out}}$) the system, effectively regulating particle flux through these sites. This can be seen well for totally asymmetric hopping, where in $\mathrm{A_{in}}$ the bulk density assumes the value $\rho_{\mathrm{bulk}} = 0.15 \pm 0.04 < \rho_{\mathrm{crit}}$ in the tunable model and $\rho_{\mathrm{bulk}} \approx \rho_{\mathrm{crit}} = 1/3$ for the ZRP. In $\mathrm{A_{out}}$ the reservoir cannot act on the bulk system, so that the bulk system is still a particle gas. For symmetric hopping, however, both phases combine and
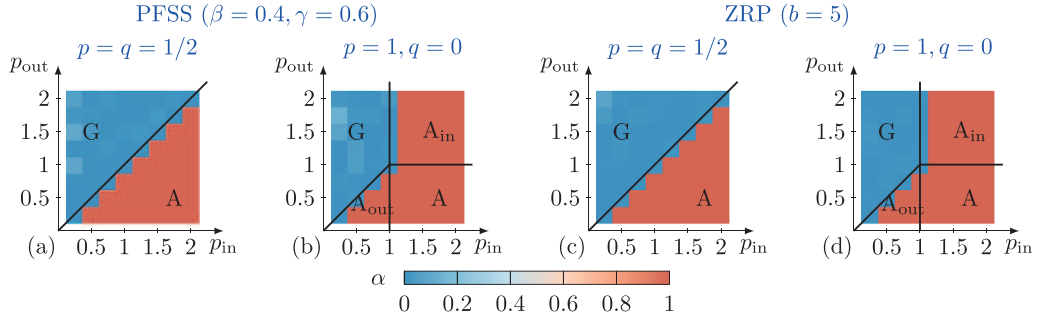
Figure 2. Scaling parameter α of the total number of particles in the ((a), (b)) ZRP-like regime for $\beta = 0.4, \gamma = 0.6$ and the ((c), (d)) ZRP for $b = 5$. Low values of $\alpha \approx 0$ indicate a stable, fluctuating total number of particles while $\alpha = 1$ shows linear growth in time.

aggregate condensates at both boundaries act on the bulk system, increasing its density to $\rho_{\mathrm{bulk}} = 0.20 \pm 0.04$ for the tunable model, still below criticality. The bulk system of the ZRP remains critical and long-lived bulk condensates sometimes emerge, which results in large values of the bulk density as shown in figure 3(c).

To understand the formation of a condensate at the influx boundary for totally asymmetric hopping a simple biased random walk in the occupation number of the first site can be considered [23]. Because the drift $p_{\mathrm{in}} - (1 + b/m)$ of the walker becomes positive for influx rates $p_{\mathrm{in}} > 1$ and sufficiently high occupation of the first site, a stable condensate can emerge at that site. In fact, we observe a power-law dependence of the waiting time on the influx rate p_{in} until the A_{in}-condensate forms after a quench to the aggregate condensate phase. This corresponds to the first-passage time of that random walk process to a sufficiently high occupation number where it has positive drift. For symmetric hopping, the argument is similar but results in a diagonal transition line to the aggregate condensate phases for $p_{\mathrm{in}} \gtrsim p_{\mathrm{out}}$ because particles may leave directly after entering. For a more detailed discussion of this argument, also with respect to partially asymmetric hopping for the ZRP, we refer to the original work of Levine *et al* [23].

The same argument can be applied to our model (2)–(4) in the regime $\beta < 1$, when the weak short-range interactions are negligible. The resulting hopping rate at the first site becomes

$$u_1 = \exp\left[\frac{1}{2}(m_1^\gamma - (m_1 - 1)^\gamma) + |m_1|^\beta - |m_1 - 1|^\beta \right], \tag{8}$$

approximated by

$$u_1 = \exp\left[\frac{1}{2}\gamma m_1^{\gamma-1} + \beta m_1^{\beta-1} \right] \tag{9}$$

for large values of m_1. This in turn approaches the value 1 for large occupation numbers m_1 as long as $\beta < 1$, that is for the entire single-site and rectangular condensate regimes of the model. The drift of the first site's occupation becomes positive for the same value of $p_{\mathrm{in}} \geqslant 1$ and yields therefore the same transition line as for the ZRP.

The formation of the aggregate condensate at the outflux boundary at site L is easily understood in the totally asymmetric case with a similar argument as above. For $p_{\mathrm{in}} < 1$ all particles eventually reach the last site L. If the removal rate is smaller than
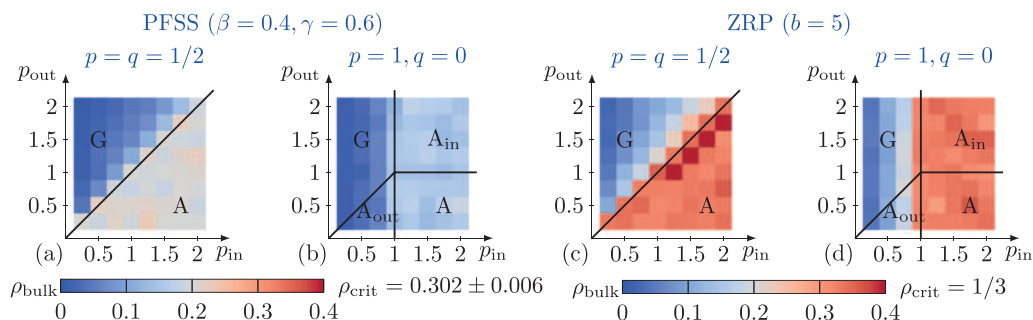
Figure 3. Bulk density ρ_{bulk} in the ((a), (b)) ZRP-like regime for $\beta = 0.4, \gamma = 0.6$ and the ((c), (d)) ZRP for $b = 5$. The critical densities for the PFSS and ZRP are $\rho_{\text{crit,PFSS}} = 0.302 \pm 0.006$ and $\rho_{\text{crit,ZRP}} = 1/3$, respectively. Except for the non-criticality of the bulk system, the dynamical phase diagram of the tunable system is to a high degree similar to that of the ZRP.

the rate of particles arriving at the site $p_{\text{out}} < p_{\text{in}}$, the drift of the occupation number m_L becomes positive and an aggregate condensate emerges.

4.2. Open boundary effects in the extended condensate regime

The goal of this section is to identify the qualitative phase structure of the described transport model depending on the strengths of particle exchange at the boundaries with respect to the considered types of boundary conditions. Within this section, the interaction parameters of the tunable transport process equation (4) are fixed at $\beta = 1.2$ and $\gamma = 0.6$, setting it into the regime of smooth parabolic condensate shapes of the periodic system [27]. The critical density for these parameters in a comparable system with $(L = 256, M \approx L)$ is $\rho_{\text{crit}} \approx 0.3$ due to finite-size effects and decreases to 0.125 ± 0.009 in the limit of large systems.

Based on the phase structure of the ZRP given in [23] and numerically reproduced for the ZRP and a short-range interaction transport model with smooth condensates in this and our own previous work [24] we expect to some extent a similar phase diagram. Therefore, to identify the phases, we continue to use the time series of the total number of particles $M(t)$, its scaling exponent α and the bulk system particle density ρ_{bulk} introduced in the previous section. An example of the total mass versus time $M(t) \sim t^{\alpha}$ for *loose* boundaries and *constant* removal along with numerically determined values of α is given in figure 4. Additionally to these quantities we record the microstates of the systems at regular intervals, so that we can compute other quantities such as the occupation number profiles that we use later.

As shown in figure 5, the scaling exponent α identifies regions with distinct values of $\alpha \approx 0$ and $\alpha \approx 1$, that is, stationary as well as linear growing total numbers of particles $M(t)$, respectively. For constant particle removal, additionally the value $\alpha \approx 0.6$ is observed on the transition line between these former regions. Together with the data for the bulk density shown in figure 6 we are able to identify candidates for gas phases with low values of $\alpha = 0$ and ρ_{bulk}, and aggregate condensate phases where $\alpha = 1$ and low values of ρ_{bulk} are observed. Additionally, a phase with stationary particle count but relatively large bulk density is found in between those for *constant* removal and symmetric hopping. To exactly identify the type of phase a system is in at any given

| | p_{in} | | | |
	0.5	1.0	1.5	2.0
p_{out} 0.5	□ 0.6079 ±0.06	□ 0.9997 ±0.0004	□ 0.9998 ±0.0004	□ 0.9997 ±0.0004
1.0	■ 0.0131 ±0.05	■ 0.6642 ±0.05	■ 1.0003 ±0.0006	■ 0.9997 ±0.0004
1.5	○ 0.0035 ±0.05	○ 0.0943 ±0.01	○ 0.6170 ±0.06	○ 0.9996 ±0.0005
2.0	● 0.0061 ±0.06	● 0.0046 ±0.05	● 0.1189 ±0.02	● 0.6215 ±0.06
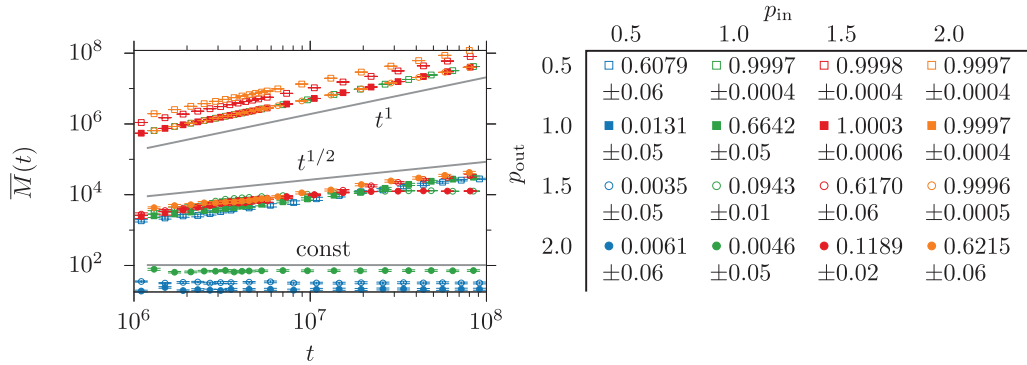
Figure 4. Average total number of particles $M(t) \sim t^{\alpha}$ for *loose* boundaries with *constant* removal of particles and symmetric dynamics ($p_{\text{in}} = q_{\text{in}}, p_{\text{out}} = q_{\text{out}}$) determined from 25 replicas. There are four distinct groups of curves: linear growth of $M(t)$ for $p_{\text{in}} > p_{\text{out}}$, approximate square root growth for $p_{\text{in}} = p_{\text{out}}$ and two groups with stationary particle numbers, both for $p_{\text{in}} < p_{\text{out}}$. The straight grey lines indicate the different observed types of scaling. The scaling parameter α as determined from the average slope in the log–log-plot in the interval $10^7 \leqslant t \leqslant 10^8$ is given right to the respective key symbol.

parameterization ($p_{\text{in}}, p_{\text{out}}$) we use graphical representations of the individual systems' evolution of microstates over time such as shown in figure 7 and averaged occupation number profiles computed from many individual trajectories shown in figure 8. Combining this information we are fully set up to identify the regions in the phase diagrams and discuss their properties in the following sections.

4.2.1. Particle gas phase (G): For the considered types of interactions at the boundaries, a particle gas phase (G) as observed for the ZRP and ZRP-like regime of the tunable model exists. Likewise it features a thin gas of particles filling the complete system. It is observed for small enough values of influx rates p_{in} and large enough outflux rates for symmetric hopping p_{out}, so that particles can directly enter and leave the bulk system. In the gas phase the system can be thought of as being part of a larger periodic system. The stationary particle density $\rho = \rho_{\text{bulk}}$ (where $\alpha = 0$ as shown in figure 5) increases with stronger drive at the boundaries towards the critical density of the steady state system as shown in figure 6. For the small system sizes we considered to obtain most of our data, the critical density is significantly influenced by finite-size effects. That is, for a small total number of particles as observed in the gas phase, the critical density $\rho_{\text{crit}} \approx 0.3$, where condensation first occurs, is considerably larger than the large system limit $\rho_{\text{crit}} = 0.125 \pm 0.009$ which is approached with increasing total particle number as shown in figure 9(a) for the ZRP and ZRP-like model and figure 9(b) for the extended condensate regime of the short-range model with $\beta = 1.2, \gamma = 0.6$. Note that the observed bulk density ρ_{bulk} for the smaller systems is above the asymptotic value of ρ_{crit}, but still below ρ_{crit} of the finite system as it should be. The values for the critical density given in figure 9(a) were determined as the background density of a periodic system with overall particle density significantly above the condensation threshold. For a very similar ZRP with hopping rates $u(m) = 1 + b/m^{\gamma}$, such finite-size effects have already been observed [34, 35].
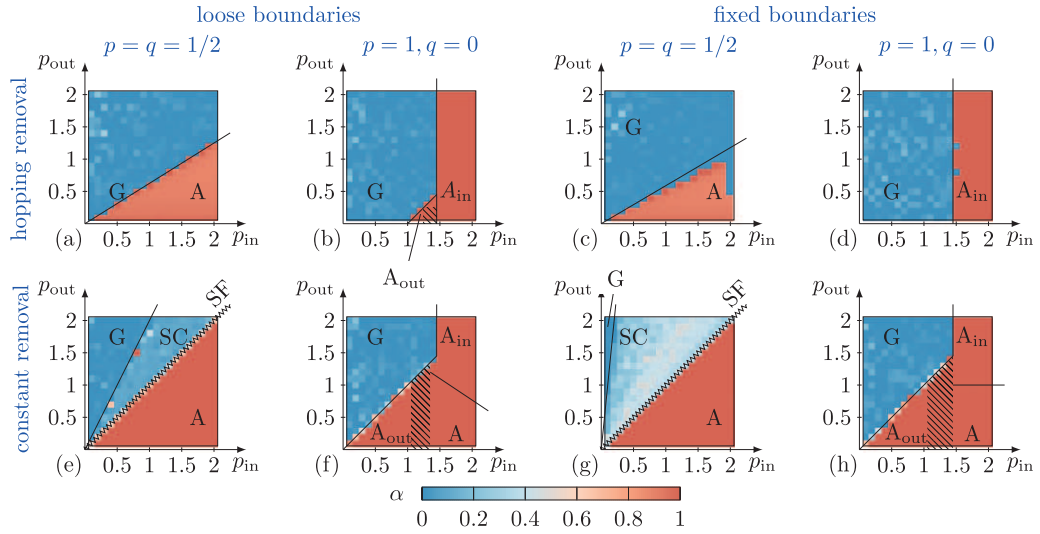
Figure 5. Average scaling exponent α of the total number of particles in the system and phase boundaries for the various types of boundary conditions. The boundary type is given by combination of the labels on the left and top margins, e.g. (f) *loose* boundaries with *constant* removal and totally asymmetric dynamics ($p = 1, q = q_{\mathrm{in}} = q_{\mathrm{out}} = 0$). The additional spanning condensate (SC) phase, which features a single stationary bulk condensate of maximal width, as well as the spanning fluid (SF) phase, where the system absorbs new particles, in panels (e) and (g) will be discussed further below in the text.

4.2.2. Aggregate condensate phases (A): For sufficiently large influx rates p_{in}, particles tend to become adsorbed at the boundary and form aggregate condensates. This is observed for any of the boundary types. As in the ZRP and the ZRP-like regime, this phase actually consists of three regions with aggregate condensates at the influx boundary, the outflux boundary and at both boundaries that exist individually for totally asymmetric hopping and mix to a single uniform region for symmetric hopping.

An example time series of an inbound aggregate condensate absorbing entering particles is shown in figure 7(b). The bulk density ρ_{bulk} as observed in figure 6 is consistently below the asymptotic value of the critical density as determined in figure 9(b). The aggregate condensates show individual shapes depending on whether they absorb inbound or outbound particles as well as on the type of boundary (*loose, fixed*) and particle removal (*hopping, constant*). The qualitative shape of *inbound* aggregate condensates A_{in} (figures 8(b), (d), (f) and (h)) closely resembles the steady state condensate shape of the model with periodic boundaries. The shape of the *outbound* condensate A_{out} (figures 8(f) and (h)) has a relatively steep increase of occupation numbers towards the boundaries but becomes almost flat when approaching the transition to A with increasing influx p_{in}. In this transition zone (hatched area in phase diagrams of figures 6(b), (f) and (h)) the aggregate condensates show significantly increased widths with respect to mass, so that merging of both aggregate condensates is observed very early compared to the region A. As a low density bulk cannot exist, these transition regions are dotted in the phase diagrams of figure 6.

The difference in condensate shapes caused by the boundary types can be seen by comparing the respective profiles row by row in figure 8 and in fact is visible also in the
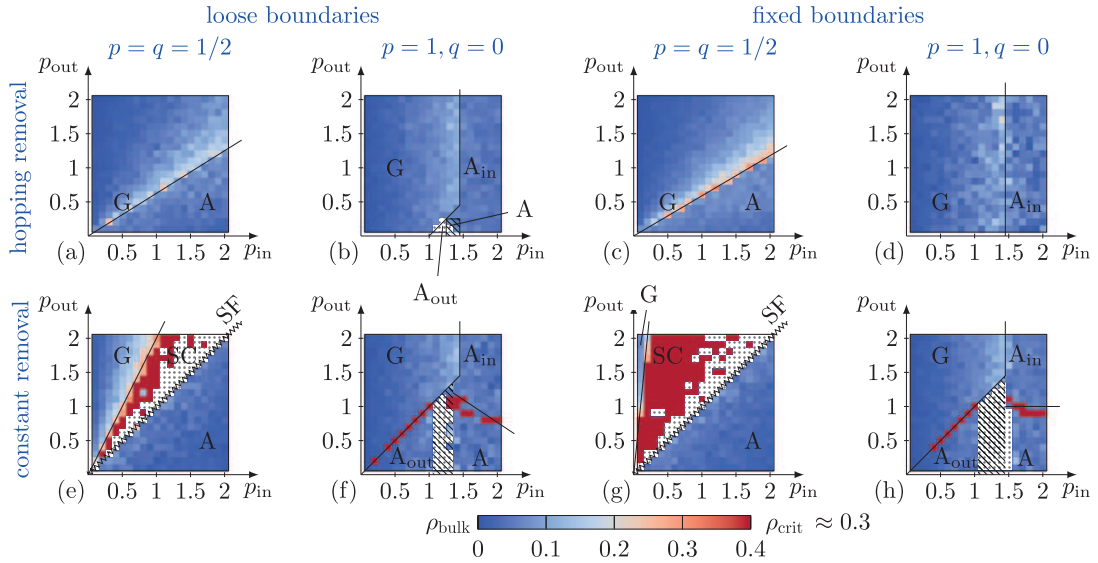
Figure 6. Particle density ρ_{bulk} in the bulk system for given boundary drives and the four considered types of open boundaries. The plot values are cut off at $\rho_{\text{bulk}} = 0.25$ to retain readability for the system with constant particle removal, where due to the large bulk condensate the density is increased by orders of magnitude. In the dotted regions, the bulk density remains undetermined as the bulk condensate has been in contact with the system boundaries in all simulated replicas. The hatched region in panels (b), (f) and (h) marks a transition region between the A_{out} and A phases. The individual plots for each boundary type are labeled as in figure 5.
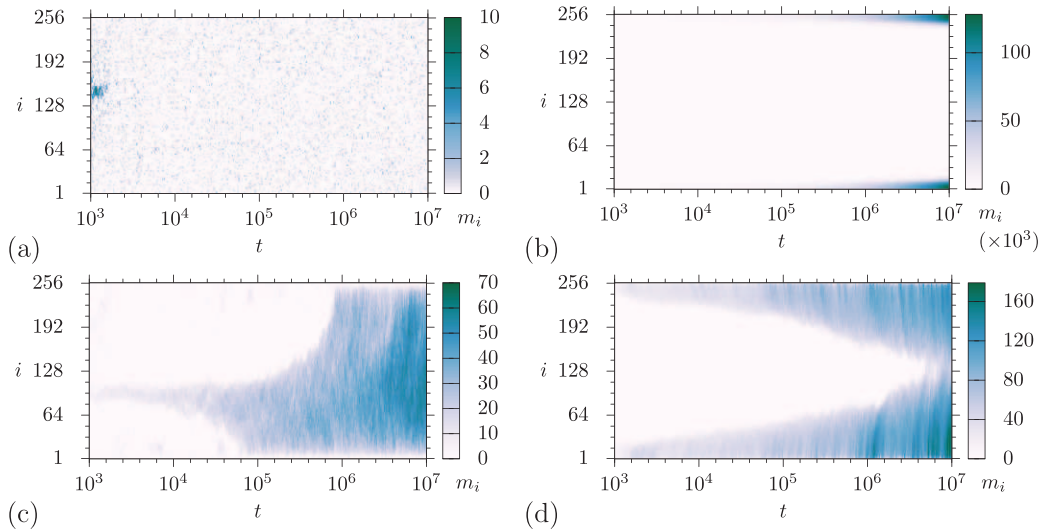
Figure 7. Example time series: (a) Gas phase (G, *loose/hopping*, $p = q = 1/2$, $p_{\text{in}} = 1.25, p_{\text{out}} = 1$), (b) boundary aggregate condensate (A_{in}, *fixed/hopping*, $p = 1, q = 0, p_{\text{in}} = p_{\text{out}} = 2$), (c) spanning bulk condensate (SC, *loose/constant*, $p = q, p_{\text{in}} = 1.25, p_{\text{out}} = 1.5$), (d) intermediate spanning fluid phase (SF, *loose/ constant*, $p = q, p_{\text{in}} = p_{\text{out}} = 2$).
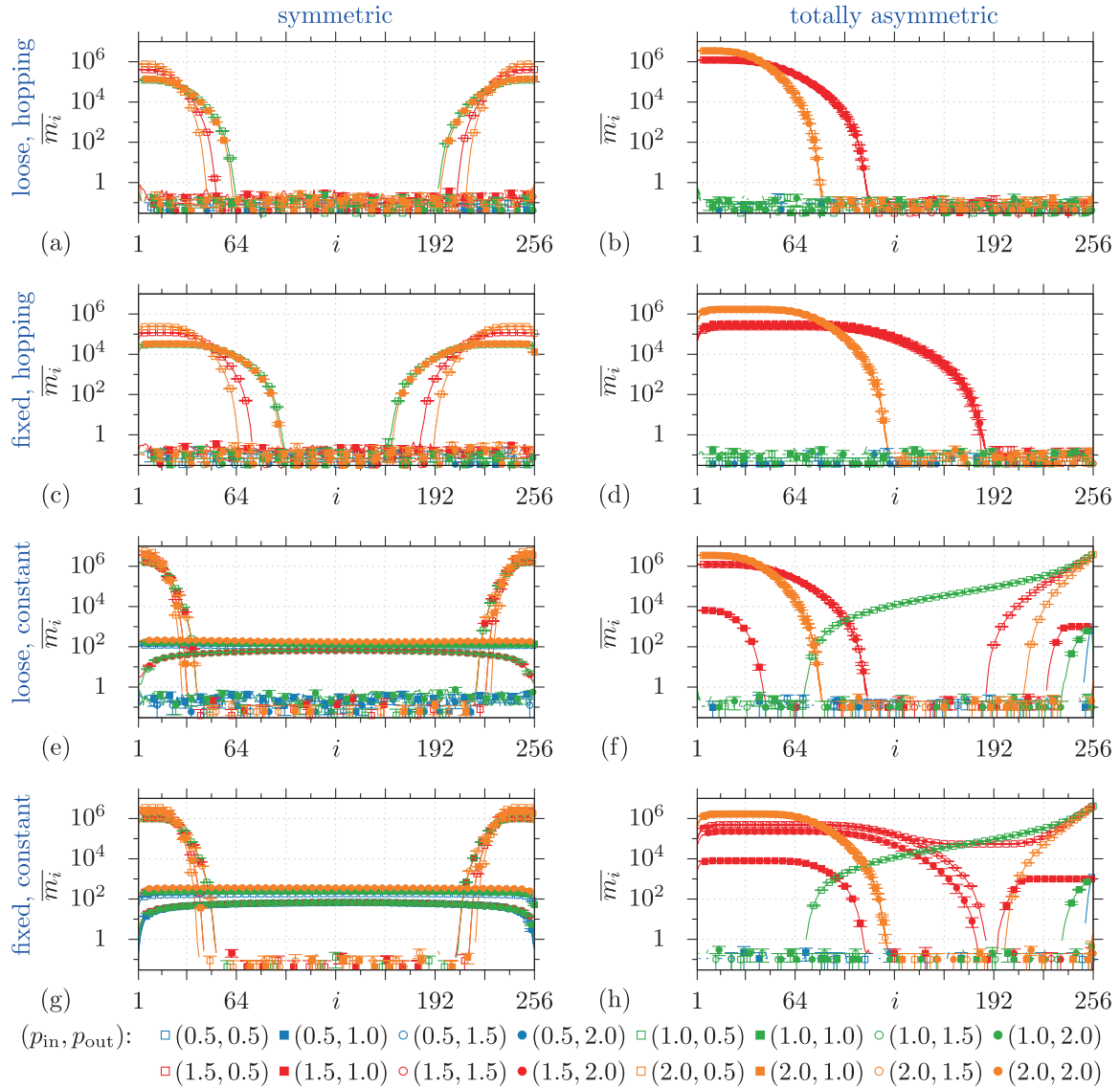
Figure 8. Average occupation number profiles m_i at simulation time $t = 10^8$ for the considered types of boundary conditions. Plot symbols refer to influx rates, colours to outflux. The boundary types are from top ((a), (b)) *loose* with *hopping* removal, ((c), (d)) *fixed* with *hopping* removal, ((e), (f)) *loose* with *constant* removal and ((g), (h)) *fixed* with *constant* removal. The left-hand side plots represent results for symmetric dynamics ($p = q = 1/2$, $p_{in} = q_{in}$, $p_{out} = q_{out}$), the right-hand side results for totally asymmetric dynamics ($p = 1$, $q = q_{in} = q_{out} = 0$). To improve readability, not all points are plotted as symbols. To compute these profiles, 25–40 trajectories were used.

large bulk condensate phase where it approaches the boundary as discussed below. For *loose* boundaries, the profile starts and ends at high occupation numbers with zero slope at the boundary. Since there is no interaction beyond the boundary, its shape is very close to one half of a steady state shape. With *fixed* boundaries, the condensate shape is forced to lower occupation numbers towards the boundaries by the interaction term with the mean-field occupation $m_\infty = 0$. Also, the maximum occupation of the condensates
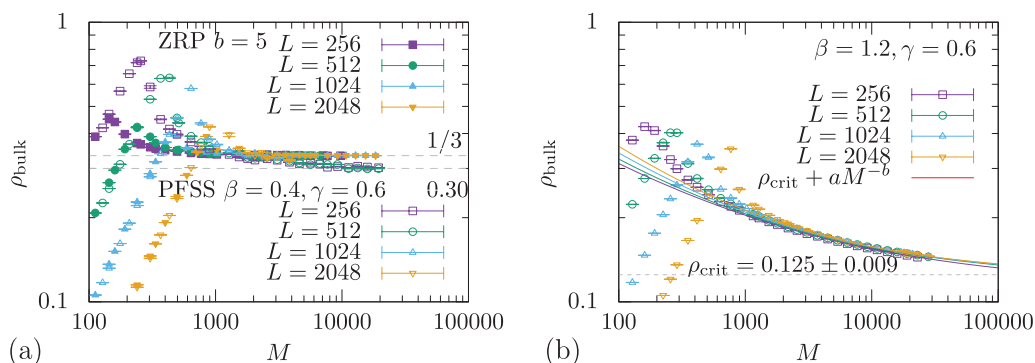
Figure 9. Finite-size effects of the critical density for low to high overall density in a closed periodic system of different sizes of $L = 256, 512, 1024$ and 2048 sites for (a) the ZRP and the effectively ZRP-like process with with $\beta = 0.4, \gamma = 0.6$ and (b) short-range interactions $\beta = 1.2, \gamma = 0.6$. For sufficiently large particle numbers M beyond the visible local maxima, condensates emerge and the bulk density ρ_{bulk} becomes the critical density ρ_{crit}. Points represent data obtained from simulation of the steady state (10^8 Monte Carlo sweeps), lines show the fitted finite-size scaling law $\rho_{\text{bulk}} = \rho_{\text{crit}} + aM^{-b}$ with $b \approx 0.40$, where the actual critical density $\rho_{\text{crit}} = 0.125 \pm 0.009$ is approached for increasing system size L and particle number M.

becomes lower which leads to increased condensate widths because the total mass of the condensates is comparably independent of *loose* or *fixed* boundaries. The mechanism of particle removal at the boundaries seems to affect the aggregate condensates only to the extent that their rates of growth are changed. *Constant* removal lets more particles escape the system and therefore results in much smaller aggregate condensates.

To estimate the slope and position of the transition line to the phase A, we perform quenches of a large number of replicas of systems to several values of the influx rate $p_{\text{in}} > p_{\text{in,crit}}$ beyond the transition line, where $p_{\text{in,crit}}$ is the critical influx rate for the given parameterization. For any value of the 'depth' $p_{\text{in}} - p_{\text{in,crit}}$ of the quench into the phase we then measure at several times the transition ratio of the gas phase

$$P_{\text{trans}}(\tau_{\text{G}\rightarrow\text{A}}) = \frac{1}{N} \sum_{i=1}^{N} H(M(t) - M_{\text{thresh}}), \tag{10}$$

where $H(x)$ is the Heaviside function, N is the number of replicas for a given value of p_{in} and $M_{\text{thresh}} = a\rho_{\text{crit}}L$ is a threshold mass (with $a > 1$) to detect the transition to the aggregate condensate phase. This transition ratio is related to the survival probability of the gas phase as $P_{\text{surv}}(\tau) = 1 - P_{\text{trans}}(\tau)$. The determined values for *loose* boundaries and *hopping* removal are given in figure 10(a). The power-law scaling of the transition time becomes evident when looking at a fixed transition ratio $P_{\text{trans}} \approx 0.5$ in figure 10(a): approximately equidistant increases of the depth of quench halve the mean waiting time to reach that transition ratio. This is illustrated in figure 10(b), which shows the scaling of the depth of quench versus the waiting time for transition of 1/2 of the replicas. The values determined for this scaling relation

$$p_{\text{in}} - p_{\text{in,crit}} \propto \tau_{1/2}^{-\kappa} \tag{11}$$

near the transition line as well as the critical influx rates $p_{\text{in,crit}}$ are given in table 1. Additionally to the considered tunable model we also considered the ZRP to check our methods. As for the PFSS, we considered the waiting time until a condensate attached to the influx boundary neglecting formation of droplets in the bulk system. We only rarely observed the case were a droplet formed away from the boundary and grew to become the aggregate condensate. We did not observe the formation of stable condensates in the bulk. We would like to suggest that the situation for bulk condensate formation here is indeed different to that of the ZRP with periodic boundaries where coarsening sets in immediately (see [4]). The phase transition could appear, when a droplet in the bulk grows fast enough to become immobile and attach to the boundary instead of diffusing or leaving the system. From our observations, the aggregate condensates in fact form at the boundary.

Using these observations of the scaling of transition times to the aggregate condensate phase, we reproduced the value of the critical influx rate $p_{\text{in,crit}} = 1$ for the ZRP (see [23]) as well as determined the scaling exponent κ, see table 1.

We would also like to point out that the exponents observed for the scaling relation of the 'depth' of quench with the transition time are within their statistical errors identical ($\kappa \approx 0.22 \pm 0.02$), although different models (tunable PFSS and ZRP), couplings (*fixed* and *loose*) or interaction at the boundary (*hopping* and *constant* removal) are considered. The physical meaning of this scaling exponent for a quench from the gas to the aggregate condensate phase is the connection of the 'depth' of the quench into the new phase to the time it takes until it manifests in the system (or the survival time of the old phase). The value of the scaling exponents here hints at a universality of this transition. Possibly related to this is the global persistence scaling exponent θ, which describes the distribution of survival times $P(\tau) \sim \tau^{-\theta}$ of the old phase after a quench to a critical point [36–38] in non-equilibrium systems. However, we would like to postpone this interesting question to future work as we could not yet address it properly.

The nature of the aggregate condensate phase is different to the regime with negligible short-range interactions (e.g. $\beta = 0.4, \gamma = 0.6$), however. This becomes clear when looking at the argument of the finite biased random walk of the occupation of the boundary sites. The hopping rate at the first site with an unoccupied neighbour does not decrease or even approach a stationary value when the occupation number m_1 increases so that a single site aggregate condensate cannot form. With a neighbour of similar occupation, however, the hopping rate u_1 has a local minimum for a non-zero occupation number, so that for this configuration of the first sites there is a positive drift of the occupation number in the random walk argument. Due to this interaction with the sites in the system, a spatially extended condensate aggregates at the boundary.

4.2.3. Spanning condensate phase (SC): With symmetric hopping and constant particle removal, an additional phase featuring a single large condensate emerges intermediate between the gas and aggregate condensate phases. The condensate spans the bulk of the system almost approaching the boundaries. As in the gas phase, the total number of particles $M(t)$ and therefore the condensate mass is stationary. This is already visible from the high value for the stationary total number of particles given in figure 4 for rates $(p_{\text{in}}, p_{\text{out}}) = (1.0, 1.5)$ and $(1.5, 2.0)$. An example time series leading to such
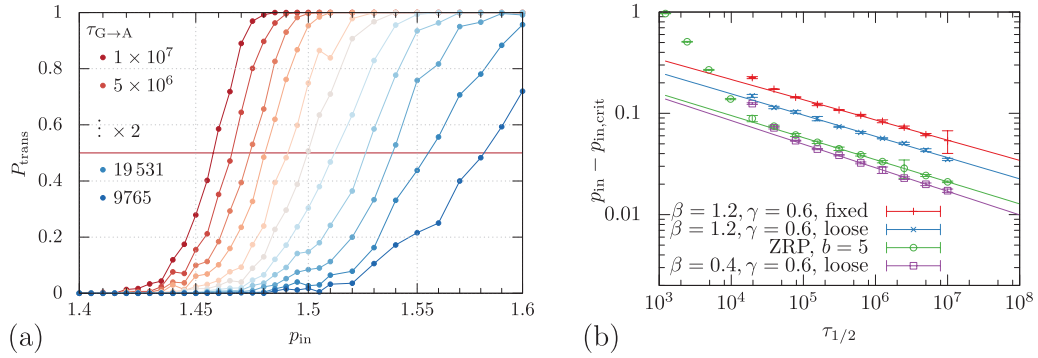
Figure 10. (a) Ratio of replicas with an emerged aggregate condensate after a waiting time $\tau_{G \to A}$ after a quench to the aggregate condensate phase (10) for influx rate values of $1.4 < p_{in} < 1.6$ and constant outflux rate $p_{out} = 1.5$ for totally asymmetric hopping. For this plot, from $N = 200$ up to 800 replicas per influx value were used with system size $L = 256$. Larger systems give qualitatively the same result. (b) Log–log plot of the excess influx rate $p_{in} - p_{in,crit}$ versus the half-value waiting time $\tau_{1/2}$, where half of the replicas have developed an aggregate condensate. Symbols represent numerical data determined from simulations of $N = 200$ system replicas of size $L = 256$, lines show the fitted scaling law (11).

Table 1. Numerically determined values for the scaling relation (11) of the quench depth $p_{in} - p_{in,crit}$ versus the waiting time $\tau_{1/2}$ to transition for $1/2$ of replicas.

	Scaling exponent κ	Critical influx rate $p_{in,crit}$
$\beta = 1.2, \gamma = 0.6$, *fixed*	0.210 ± 0.064	1.426 ± 0.018
$\beta = 1.2, \gamma = 0.6$, *loose*	0.200 ± 0.027	1.459 ± 0.013
$\beta = 0.4, \gamma = 0.6$, *loose*	0.233 ± 0.031	1.0337 ± 0.0038
ZRP, $b = 5$	0.218 ± 0.014	1.0055 ± 0.0024

Note: These values are determined for totally asymmetric hopping and fixed outflux rate $p_{out} = 1.5$, where the critical influx rate does not depend on p_{out}.

a spanning bulk condensate is shown in figure 7(c). The resulting average occupation profile for large times is shown in figures 8(e) and (g). There it is visible that towards the phase boundary to the aggregate condensate phase the bulk condensate starts to touch the boundary sites. This becomes clear in figures 6(e) and (g) where the dotted region indicates that the measurement of the bulk density as defined in equation (7) cannot be achieved because the bulk does not exist.

To understand why this additional phase occurs with the *constant* removal mechanism, we suggest that for single particles at the boundary as it occurs in the gas phase, the removal rate is much lower than with the *hopping* removal mechanism. With asymmetric hopping this leads to emergence of an outward boundary aggregate condensate (A_{out}) as evident from figures 6(f) and (h). For symmetric hopping, however, this leads to an increase of the bulk density above the critical density and thus the formation of a bulk condensate. This condensate then absorbs particles until its stable maximum size is reached. When the particle influx rate p_{in} becomes large enough to create aggregate condensates, the bulk condensate connects to the boundaries resulting in a flat occupation profile. We mark this transition with a zig–zag line denoted as spanning fluid

(SF) phase in figures 5 and 6. The total number of particles in this transitionary state grows roughly with $\alpha \approx 0.6$ as shown in figures 4 and 5.

5. Conclusion

We systematically studied the effects of open boundaries and external drive in a stochastic transport process with tunable short-range interactions [11, 12] far from equilibrium. To do so in a meaningful and systematic way we proposed four different boundary types distinguished by the type of interaction and the mechanism of particle removal at the boundary. The interaction at *loose* or *fixed* boundaries reflects the non-existence or existence of an interaction term with a mean-field occupation across the boundary site. For leaving particles, additional to *hopping* removal, we propose *constant* removal for reasons of the symmetry of particle exchange. We considered the four types of open boundaries generated by combinations of these properties and determined the respective phase diagrams for both symmetric and totally asymmetric hopping dynamics.

We successfully applied the direct KMC technique, a continous-time Monte Carlo method to the system to control the unbounded values of the hopping rate of the chosen dynamics for $\beta > 1$ where in the steady state of the closed (periodic) system extended condensates of smooth parabolic shape form. This, however, also mitigates the need to artificially formulate update sweeps that coordinate regular particle hops with particle injections and removals because all events can be treated equally only according to their rates leading to a uniform time scale.

For negligible strength of the short-range interaction ($\beta < \gamma$) we found a phase diagram that is essentially equivalent to that of the ZRP condensation model (1) as discussed in [23]. A homogeneous particle gas phase and an aggregate condensate phase make up the phase diagram. The transition mechanism between these can be understood the same way as for the ZRP.

When the short-range interactions become important ($\beta > 1$) we find an enriched phase structure. The particle gas phase is identical to that in the prior models. In the aggregate condensate phases, however, spatially extended condensates emerge at the boundary sites with envelope shapes that adapt to the predominant flux of particles in or out of the system in case of asymmetric dynamics. The interaction at *loose* or *fixed* boundaries, while not changing the phase structure qualitatively, does have a significant effect on the transition lines between phases as well as the properties in the aggregate condensate phases. In the case of *fixed* boundaries, this is very obvious in the deformation of the aggregate condensates at the boundary sites. With the constant rate particle removal mechanism, however, we observed the emergence of a new intermediate phase featuring a dominant bulk condensate between the particle gas and aggregate condensate phases. To obtain a precise value for the critical influx rate that separates phases G and A_{in} for totally asymmetric hopping, we analyzed survival times of the gas state for different quenches to A_{in}. An interesting observation in this analysis was the identity of the scaling exponents of the relation between distance to the transition line and half-value survival time across different models, coupling strengths and considered boundary types. While we could not yet identify the cause of this scaling, it appears to

be a universal property for this type of phase transition. As a future project it would be interesting to work out its possible relation to the global persistence scaling.

Acknowledgments

References

[1] Spitzer F 1970 *Adv. Math.* **5** 246–90
[2] Evans M R 2000 *Braz. J. Phys.* **30** 42–57
[3] Godrèche C 2003 *J. Phys. A: Math. Gen.* **36** 6313–28
[4] Godrèche C and Luck J M 2005 *J. Phys. A: Math. Gen.* **38** 7215–37
[5] Großkinsky S, Schütz G M and Spohn H 2003 *J. Stat. Phys.* **113** 389–410
[6] Beltrán J and Landim C 2011 *J. Stat. Phys.* **140** 1065–114
[7] Beltrán J and Landim C 2012 *J. Stat. Phys.* **149** 598–618
[8] Landim C 2014 *Comm. Math. Phys.* **330** 1–32
[9] Evans M R and Hanney T 2005 *J. Phys. A: Math. Gen.* **38** R195–240
[10] Evans M R, Hanney T and Majumdar S N 2006 *Phys. Rev. Lett.* **97** 010602
[11] Wacław B, Sopik J, Janke W and Meyer-Ortmanns H 2009 *Phys. Rev. Lett.* **103** 80602
[12] Wacław B, Sopik J, Janke W and Meyer-Ortmanns H 2009 *J. Stat. Mech.* P10021
[13] Bogacz L, Burda Z, Janke W and Wacław B 2007 *Chaos* **17** 26112
[14] Wacław B, Bogacz L, Burda Z and Janke W 2007 *Phys. Rev.* E **76** 46114
[15] Wacław B, Sopik J, Janke W and Meyer-Ortmanns H 2009 *J. Phys. A: Math. Theor.* **42** 315003
[16] Schütz G M 2000 Exactly solvable models for many-body systems far from equilibrium *Phase Transitions and Critical Phenomena* vol 19, ed C Domb and J Lebowitz (London: Academic) pp 1–251
[17] Schadschneider A, Chowdhury D and Nishinari K 2011 *Stochastic Transport in Complex Systems* (Amsterdam: Elsevier)
[18] Katz S, Lebowitz J and Spohn H 1983 *Phys. Rev.* B **28** 1655–8
[19] Katz S, Lebowitz J and Spohn H 1984 *J. Stat. Phys.* **34** 497–537
[20] Evans M R and Wacław B 2014 *J. Phys. A: Math. Theor.* **47** 095001
[21] Evans M R and Wacław B 2015 *J. Stat. Mech.* P09005
[22] Popkov V and Schütz G M 1999 *Europhys. Lett.* **48** 257–63
[23] Levine E, Mukamel D and Schütz G M 2005 *J. Stat. Phys.* **120** 759–78
[24] Nagel H, Labavić D, Meyer-Ortmanns H and Janke W 2014 *Phys. Procedia* **57** 77–81
[25] Nagel H, Meyer-Ortmanns H and Janke W 2015 *Europhys. Lett.* **111** 30001
[26] Białas P, Burda Z and Johnston D A 1997 *Nucl. Phys.* B **493** 505–16
[27] Ehrenpreis E, Nagel H and Janke W 2014 *J. Phys. A: Math. Theor.* **47** 125001
[28] Gillespie D T 1976 *J. Comput. Phys.* **22** 403–34
[29] Gillespie D T 1977 *J. Phys. Chem.* **81** 2340–61
[30] Bortz A B, Kalos M H and Lebowitz J L 1975 *J. Comput. Phys.* **17** 10–8
[31] Chatterjee A and Vlachos D G 2007 *J. Comput. Mater. Des.* **14** 253–308
[32] Schulze T P 2002 *Phys. Rev.* E **65** 036704
[33] Gibson M A and Bruck J 2000 *J. Phys. Chem.* A **104** 1876–89
[34] Chleboun P and Grosskinsky S 2010 *J. Stat. Phys.* **140** 846–72
[35] Evans M R, Majumdar S N and Zia R K P 2006 *J. Stat. Phys.* **123** 357–90
[36] Majumdar S N, Bray A J, Cornell S and Sire C 1996 *Phys. Rev. Lett.* **77** 3704–7
[37] Majumdar S N 1999 *Curr. Sci.* **77** 370–5
[38] Bray A J, Majumdar S N and Schehr G 2013 *Adv. Phys.* **62** 225–361